Laser Scanner and Terrestrial Surveying Applied to Gravitational Deformation Monitoring of Large VLBI Telescopes' Primary Reflector

Pierguido Sarti[1]; Luca Vittuari[2]; and Claudio Abbondanza[3]

Abstract: Laser scanning surveys were performed on the primary mirror of the very long baseline interferometry (VLBI) telescopes situated at Medicina and Noto observatories, with the specific purpose of investigating (1) gravity deformation patterns of the radio telescopes' primary reflector and (2) the magnitude and relative variations of focal length as the antennas are steered in elevation. Both instruments have Azimuth-Elevation mounts and have 32 m parabolic mirrors which were surveyed in steps of 15° spanning the 90–15° elevation range. The scanning sessions were performed from two standpoints using a GS200 Trimble-Mensi; the sampling interval was set to 2 cm at a distance of 15 m. The complete surface of the main reflector at every elevation position was obtained by merging the two separate point clouds acquired from the two standpoints; each elevation is represented by at least 1.3 millions points. The merged clouds were compared for determining relative deformation patterns and magnitude. As the elevation decreases from 90−15°, the edges of the primary mirror of both telescopes fold in by a couple of cm. A least-squares adjustment was applied to point clouds corresponding to different elevations aimed at estimating the parameters of the rotational paraboloids that better fit the experimental data. This led to estimate the focal length variations induced by the structure deformative behavior. The focal lengths of the best-fit surfaces were compared. Their largest variation is found to be 2.5 cm at Medicina, between the 90° and the 15° positions. The clouds were also used to attempt a direct computation of the incoming radio signal's path length variation due to primary reflectors' deformations. Finally, two Leica total stations, a TDA5005 and a TC2003, were used to perform a survey of the local ground control network and of some selected targets placed on the edge of the dish. The comparison of the distances determined with the two terrestrial surveying methods (laser scanner versus triangulation and trilateration) highlights a statistically significant scale factor of about 1.0005 ± 0.0002, being the laser estimates smaller than those obtained with total stations. This study proves that laser scanners can be efficiently used to determine gravitational influences on large VLBI telescopes' primary reflectors: deformation patterns are clearly and reliably depicted, focal length and incoming radio signal path variations are precisely quantified.

DOI: 10.1061/(ASCE)SU.1943-5428.0000008

CE Database subject headings: Lasers; Telescopes; Deformation; Surveys.

Introduction

The Italian very long baseline interferometry (VLBI) project started in the mid-1970s when the Istituto di Radioastronomia of the Consiglio Nazionale delle Ricerche planned the construction of three identical VLBI radio telescopes on different parts of Italy, aimed at developing radioastronomic research and at extending the VLBI geodetic network for geodynamics applications (Setti 2006). A lack of available funding led to an important reconsideration of the project: it was eventually modified withdrawing the construction of the radio telescope in Sardinia. The situation changed in the early 1990s. A geodetic 22-m VLBI telescope started its operation in Matera and the construction of the Sardinia telescope was reconsidered and refinanced. This latter radio telescope is designed as an azimuth-elevation (AZ-EL) 64-m dish whose technical characteristics can be found in Olmi and Grueff (2006). It should be completed and operative by the end of 2009.

The other Italian VLBI radio telescopes were regularly built and completed during the 1980s. They are twin AZ-EL mount 32-m dish (Fig. 1) and the first geodetic observation took place in 1987 in Medicina (Tomasi et al. 1988) while Noto's geodetic observations began in 1989 (Tomasi 1993). Ever since, both telescopes have actively participated in the observations of the international VLBI network; in particular, the geodetic activities are nowadays coordinated by the International VLBI Service (see e.g., Schlüter and Behrend 2007), which has been greatly contributing in widely and uniformly promoting the scientific as well as the technological development of VLBI technique.

Both observatories are International Terrestrial Reference Frame (ITRF) colocation sites where global positioning system and VLBI intertechnique eccentricities are maintained and regularly surveyed using an indirect method based on high precision terrestrial observations (Sarti et al. 2004). The eccentricities are provided in SINEX (solution independent exchange) format with a full variance covariance matrix and both tie vectors have

[1]Researcher, Institute of Radioastronomy, INAF, via P. Gobetti, 101, Bologna 40129, Italy (corresponding author). E-mail: p.sarti@ira.inaf.it

[2]Associate Professor, DISTART, Univ. of Bologna, v.le Risorgimento, 2, Bologna 40131, Italy. E-mail: luca.vittuari@mail.ing.unibo.it

[3]Institute of Radioastronomy, INAF, via P. Gobetti, 101, Bologna 40129, Italy. E-mail: c.abbondanza@ira.inaf.it

Note. This manuscript was submitted on October 1, 2008; approved on March 16, 2009; published online on March 27, 2009. Discussion period open until April 1, 2010; separate discussions must be submitted for individual papers. This paper is part of the ***Journal of Surveying Engineering***, Vol. 135, No. 4, November 1, 2009. ©ASCE, ISSN 0733-9453/2009/4-136–148/$25.00.

Fig. 1. 32-m AZ-EL VLBI radio telescope at Medicina; the VLBI telescope in Noto has the same design, structure, and dimensions

been used in the most recent and final computation of ITRF2005 (Altamimi et al. 2007).

Local ties are essential for intertechnique combinations; nevertheless, combinations of reference frames defined by different techniques as well as combined solutions performed on common parameters highlight significant discrepancies between the local tie and the space geodetic observations (e.g., Ray and Altamimi 2005; Altamimi et al. 2007; Krügel et al. 2007; Thaller et al. 2007). These discrepancies may have different origins; a crucial role is played by the stability of the reference points (RPs) of the different colocated space geodetic instruments. A particular source of instability which affects the RP of large VLBI telescope is gravity: it is capable of inducing deformative patterns in the telescope structure which cannot be neglected when aiming at accurately locating the RP's position. The conventional position of the RP is defined for each space geodetic instrument but its physical realization during the space geodetic observations, i.e. the antenna's or receiver's phase center, may vary considerably (see e.g., Sarti and Angermann 2005; Leinen et al. 2007). This latter may be regarded as electrical RP and it identifies the point where space geodetic observable is acquired. In order to connect conventional and electrical RPs the International VLBI Service (IVS) standard analysis procedure nowadays requires to add an elevation dependent contribution of the offset O, possibly existing between the fixed and the moving axis of the telescope: if $O \neq 0$ its projection along the line of sight must be added to the VLBI signal path. This implies that the effect of gravity on the telescope structure is neglected: gravitational deformations are not taken into account and the signal path length is not varied accordingly. They are believed to balance themselves or to have a negligible impact on signal path variations (Gendt et al. 2007). This statement is not proved to be true and gravity may originate significant elevation dependent changes in VLBI signal path, especially in large VLBI telescopes, and may be the cause of VLBI telescope's RP instability and, consequently, discrepancies between local ties and space geodetic observations. Gravitational deformations do remain complex to investigate; since the very beginning of VLBI observations, the action of gravity on VLBI telescopes' structures has been acknowledged as a factor which corrupts VLBI geodetic observations and degrades the accuracy of estimated geodetic parameters (Carter et al. 1980).

Clark and Thomsen (1988) identified the critical contribution of three gravity dependent parameters to signal path length variations: the components along the line of sight of (1) the displacement of the receiver; (2) the displacement of the primary mirror (essentially described by its vertex's position); and (3) the change of focal length. This study focuses on the latter: focal length is strictly related to the shape of the primary mirror and its response to gravitational deformations. Any elevation dependent change of the main reflector's topology modifies the antenna optics and corrupts the observations.

Clark and Thomsen (1988) investigated the signal path variations of the Fairbanks (Alaska) antenna: in order to quantify the contributions of the three different effects, they used a finite-element model (FEM) of the antenna. Photogrammetry and holography are different methods that have been successfully applied to gravitational deformation monitoring (see e.g., Subrahmanyan 2005; Rochblatt and Seidel 1992).

Alternatively to the previous methods, this paper describes the use of laser scanning technique for surveying the main reflector of Noto and Medicina VLBI telescopes. The surveys were carried out in September 2005 with the aim of studying the gravitational deformation patterns of the primary mirrors and of determining their focal length at six different pointing elevations. The laser scanner (LS) data were integrated by other terrestrial observations, in particular triangulation and trilateration, performed on common points and on the local ground control network. They were originally performed to directly link the local ground control network and the LS observations, thus providing a common reference frame in which the deformation patterns could be compared and eventually connected to the VLBI RP. Nevertheless, the considerable number of transformations needed to connect the different frames that are defined in the surveys and the large uncertainties on the positions of the common points prevented an effective calculation of the absolute deformation patterns.

VLBI Radio Telescopes at Medicina and Noto

The VLBI telescopes located at Medicina and Noto are twin 32-m Cassegrain antennas characterized by a frequency operability ranging from 1.4–22 and 0.3–43 GHz, respectively. They have an AZ-EL mount with non intersecting axis; the project design offset between the fixed azimuth axis and the moving elevation axis is $O=1.829$ m. Depending on the observing frequency, receivers are placed in the primary or secondary focus position. In the latter case, the hyperbolic secondary mirror reflects the incoming wavefront toward the Cassegrain focus. The focus positions can be selected by moving the subreflector: it can be retracted, so as to access the receivers placed in the primary focus or can be shifted and rotated, so as to ensure the reflection of the incoming signal toward the nine adjacent available focal positions near to the primary reflector's vertex.

The 32-m primary mirrors are realized with 240 aluminum panels mounted on reticular structures which hold and support the primary reflector, the receiving systems, the quadrupode and the subreflector. Detailed and complete technical descriptions of both telescopes can be found at the home page of the Istituto di Radioastronomia (http://www.ira.inaf.it).

Geodetic observations are performed at S and X-bands (2.3 and 8.4 GHz, respectively) and the corresponding receivers are located in primary focus position. In order to maintain high efficiency, reduce antenna gain degradation and allow higher frequency observations, it is important to know how the different parts of the VLBI telescope deform under the effect of gravity.

The paraboloidal shape of the primary mirror, by definition, coherently reflects the incoming wavefront toward the focal point. The theoretical surface of a rotational paraboloid with vertex in (0,0,0), its rotation axis identified by the Z-axis and having focal length f, is described by

$$Z = \frac{X^2 + Y^2}{4f} \tag{1}$$

Medicina and Noto VLBI telescopes have a nominal focal length $f = 10.2590$ m.

Gravity constantly acts on the telescope's structure and deforms it depending on the pointing position of the dish during the observation. Differential deformations occur when the elevation changes, while azimuth rotations do not significantly modify the telescope's structure. According to Clark and Thomsen (1988), gravitational deformations of the telescope's structure originate a variation in the signal path length which can be described as

$$\delta dL = \alpha_f dF + \alpha_v dV + \alpha_r dR \tag{2}$$

where dF=variation of the focal length; dV=movement of the vertex of the dish; and dR=movement of the receiver, all considered along the line of sight. The magnitude of the first and second terms are strictly related to the deformation of the primary mirror while the third term dR, when the receivers are placed in primary focus position, is connected to the deformations that affect the quadrupode. Coefficients α_f, α_v, and α_r depend on the dimension and structure of the telescope and contribute to the definition of the total signal path modification (see Clark and Thomsen 1988).

Focal length (as well as receiver's and vertex's positions) depends on the pointing elevation of the telescope: the primary mirror's surface is deformed by gravity and modifies the shape of the main reflector which, accordingly, reflects the incoming wavefront in a different focal point. In order to counter the effect of gravity on the primary mirror, Noto VLBI telescope was upgraded and equipped with an active surface in 2001 (Orfei et al. 2004). The panels that cover the primary mirror can be moved through electromechanical actuators. Each panel moves according to an elevation dependent correction model: values are listed in a file and represent the translations that must be applied to the panels for restoring the ideal parabolic shape of the primary mirror.

High frequency radioastronomy observations rely on the possibility to maintain the parabolic shape of the primary mirror; therefore, precise geometric corrections introduced by active surfaces are fundamental for ensuring the coherence of the signal and maximizing the antenna gain. The position of the receiver during the observations is also crucial. The amplitude of the antenna voltage radiation pattern is maximized by placing it in the point were the majority of the incoming signal concentrates, depending on the variations induced by gravity. At this location, in order to determine the positions of the receiver that maximize the antenna gain as the elevation of the antenna varies, a calibration procedure is performed. Some selected radiosources are observed while the receiver is shifted and moved back and forth along the line of sight; the procedure aims at determining the receiver's positions that maximize the antenna voltage radiation in the range of elevations which the antenna can be steered at. The elevation dependent translations along the line of sight to be applied to the receivers during the observations were computed for the S/X-bands receiver in Noto and for the K-band receiver in Medicina; in the pointing elevation range of 0–90°, the primary focus receivers must be shifted by 1 cm in Noto and almost 2 cm in Medicina. The telescopes are twins and should not exhibit such a different behavior; possible explanations are given in the next section. It is very important to underline that under no circumstances is the position of the S/X receivers actively changed during geodetic VLBI observations: elevation dependent movements of the receivers along the line of sight straightforwardly map into elevation dependent modifications of the signal path and must therefore be avoided. Furthermore, it should be highlighted that the translations to be applied to the receivers located at the primary focus are influenced by the deformation of the quadrupode and the deformation of the main reflector: they determine the terms dR and dF of Eq. (2). The antenna gain is not affected by the term dV since it does not depend on the observing position of the dish along the line of sight.

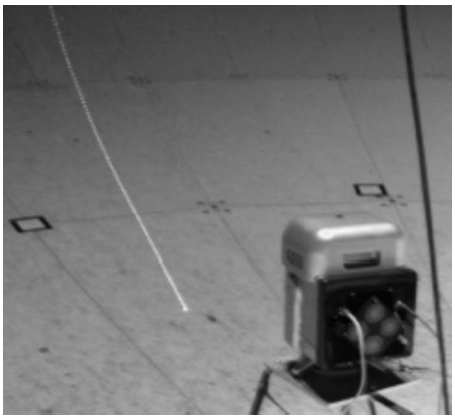

Fig. 2. GS200 Trimble-Mensi laser scanner operating on the primary mirror surface of the Noto VLBI telescope

In order to determine the three terms of Eq. (2), Clark and Thomsen (1988) used a FEM. This latter approach is efficient provided that the FEM accurately represents the telescope structure. The model itself is extremely complex and the static as well as the structure schemes must be properly chosen; it is crucial to adopt the right finite elements and relate them in such a manner that the physics of the structure can be accurately reproduced. Any mistake affecting the model would lead to wrong results and wrong deformations that would be very difficult to trace. As an alternative to FEM based investigations, we have tested terrestrial surveying: the next two sections describe the laser scanning and trilateration and triangulation measurement approaches.

Laser Scanning Surveys

Surveys Setup

The instrument that was used to perform the surveys in Medicina and Noto is a GS200 Trimble-Mensi LS (Fig. 2). Its measuring approach is based on the time-of-flight (TOF) determination. It can record up to 5,000 points' positions per second and its best positioning accuracy attains the value of 1.5 mm at 50 m (see http://www.trimble.com/gs200.shtml).

An alternative to TOF is phase measurement approach which can be applied to surveys where ranges do not exceed 100 m with precisions similar to those attainable with TOF (Fröhlich and Mettenleiter 2004). LSs that use the optical triangulation (OT) method ensure higher performances and a more accurate determination of points' positions. Unfortunately, such an approach can

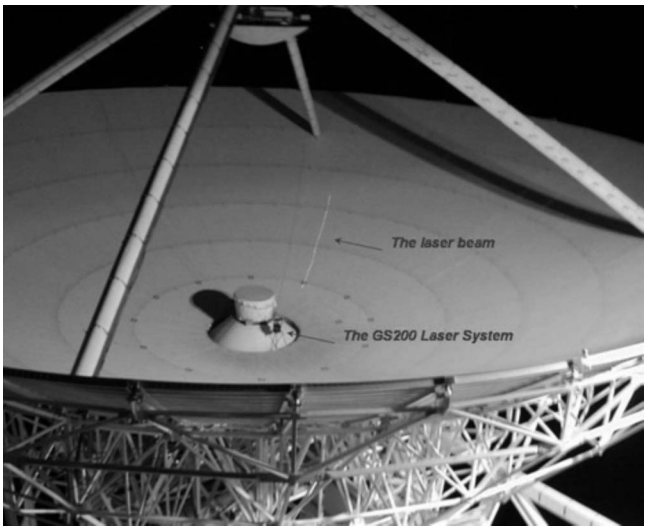

Fig. 3. Laser scanner night session at Noto. The instrument stands on one side of the receivers' shelter (the cylinder at the center of the paraboloid).

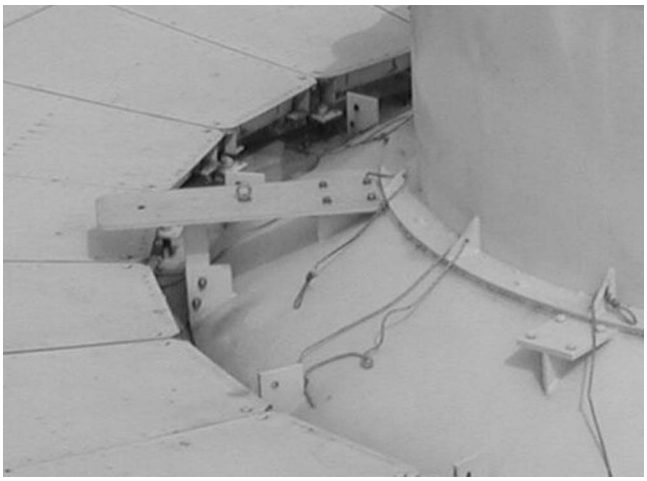

Fig. 4. Support of the laser scanner inside the Medicina primary reflector; on the right, a part of the cylindrical shelter of the Cassegrain receivers is visible

only be applied to short range measurements, typically well within 10 m. The precisions that can be obtained on relatively small objects is extraordinary; several examples are represented by the applications in the field of historical and cultural heritage documentation, where submillimeter precisions can be obtained on details or small size objects (e.g., Pieraccini et al. 2001; Yemez and Wetherilt 2007).

In principle, the shape of the VLBI telescopes' primary mirror should be determined at the submillimeter level; thus, an OT LS would have been the best solution. Nevertheless, a number of aspects had to be taken into account and evaluated before making a final decision. Primarily, the dimension of the object to be surveyed and the suitable measurement approach: the dish size is 32 m and OT LS do not ensure the best performances on such a large object. A second fundamental aspect was related to the actual range of renting opportunities that we were offered: the LS had to be available for a couple of weeks, the rent had to be reasonably priced and its nominal accuracy as high as possible. These aspects concurred to adopt the GS200 LS.

The performances of the LS on the surface of the primary mirror, its repeatability and the quality of successive scans were evaluated before the surveys, using a sample surface whose composition, in terms of material and paint, was identical to that of the panels of the telescope. The sample was moved in different positions so as to reproduce distances and angles similar to those eventually found in field observations; in particular, those measurements performed at grazing angles to the surface of the main reflector represented a critical aspect of the survey that had to be tested in advance. The instrument's performances on the test surface were satisfactory, ensuring a repeatability of the same order of magnitude of the LS nominal precision; therefore, the GS200 Mensi was eventually adopted for the surveys.

In order to reduce the impact of refractivity and diminish the air turbulence effect on the LS performances, the scanning sessions were performed during night time (Fig. 3). In total, at each observatory were realized twelve partially overlapping scans. The surface of the primary mirror was surveyed at six elevations (90°, 75°, 60°, 45°, 30°, and 15°) from two different standpoints F1 and F2. A one night session ensured the time necessary to complete six elevations scans from one standpoint: therefore, two nights are required to fully survey the main reflector.

Unfortunately, in Noto a data loss occurred during the scans from F2 at elevations 75° and 60°: the corresponding data and results are consequently missing. The mechanical properties of the LS would permit a full survey of the primary mirror from a single standpoint located near the vertex of the dish: the instrument rotates in azimuth and elevation, spanning angles of 360° and 60°, respectively. Nevertheless, the presence of the cylindrical Cassegrain receivers' bays (see Fig. 3) forced us to carry out the survey from two separate positions and acquire two partially overlapping scans that were merged later into a single cloud. The design and realization of the standpoints aimed to ensure a firm and stable support for the LS at any elevation of the dish (Fig. 4). The characteristics of the primary mirror surface in terms of symmetry, shape, and dimensions required the use of six targets that could be clearly identified on both scans and could be used as common points to align the two clouds and merge them into one. These spherical targets are identified with a capital "S" in Fig. 5 and were surveyed applying a denser sampling interval when compared to the surface of the mirror: a point every 3 mm versus the usual sampling interval of a point every 20 mm at 15 m.

Data Processing, Postprocessing, and Results

A filtering procedure was applied on every scan, aimed at identifying and removing all the points that were measured during the survey but that did not belong to the primary mirror surface. As previously stated, the surface of the mirror is made by 240 panels; a small gap (approximately 1 cm) between the panels often caused the laser beam to hit the supporting reticular structure underneath the panels or other parts of the telescope structure. To a large extent, these outliers were manually removed and the resulting sets of points were saved as new working data set.

Subsequently, the alignment and merging phase of the scanned points acquired from F1 and F2 (Fig. 6) were fundamental in order to obtain a unique set of points for every elevation. In this particular case it was neither an easy nor trivial task; the peculiarities of the VLBI primary mirror, specifically its homogeneous

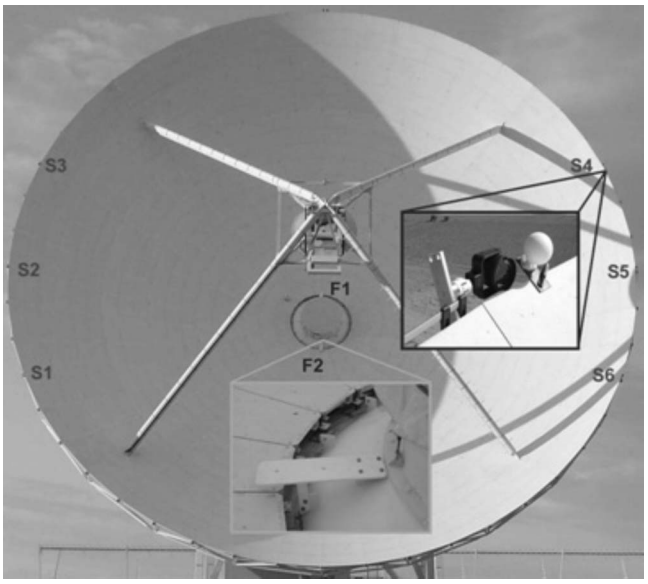

Fig. 5. Medicina VLBI telescope: the standpoints F1 and F2 are symmetrically located with respect to the Cassegrain receivers' shelter. The location of the spheres and the retroreflecting prism is identified by the letter "S." The inset shows the relative positions of the two targets. Spheres were observed with the laser scanner and triangulation, prisms were triangulated and trilaterated.

color and its regular shape, prevented a straightforward and easy identification of features which could be easily used to rotate and translate one set onto the other. The homogeneity of the entire surface and its smooth profile prevented a differentiation of the surface within the overlapping areas in the scanning sessions performed from standpoints F1 and F2. The six spheres placed at the edge of the dish were specifically installed and surveyed for providing tie points: detailed scans of the surface of the spheres provide a set of points from which it is easy to estimate, possibly using specific LS software suites, the coordinates of their centers.

The alignment phase of the two scanned points was critical and it was performed applying the iterative closest point (ICP) algorithm (Besl and McKay 1992).

Each complete cloud contains almost 1.4 millions points in Medicina and 1.9 millions in Noto; they represent the deformed surface of the primary mirror at different elevations and they characterize the behavior of the dish under the effect of gravity as the antenna is steered to different elevation positions. In order to associate each cloud to a best-fit paraboloid, a special-purpose

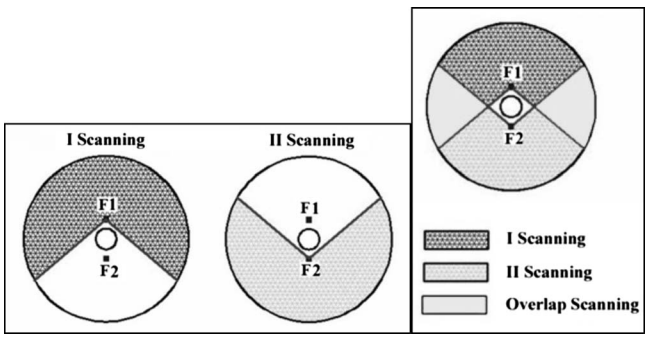

Fig. 6. Example of the two sets of points scanned from the standpoints F1 and F2 at six different elevations of the VLBI telescope

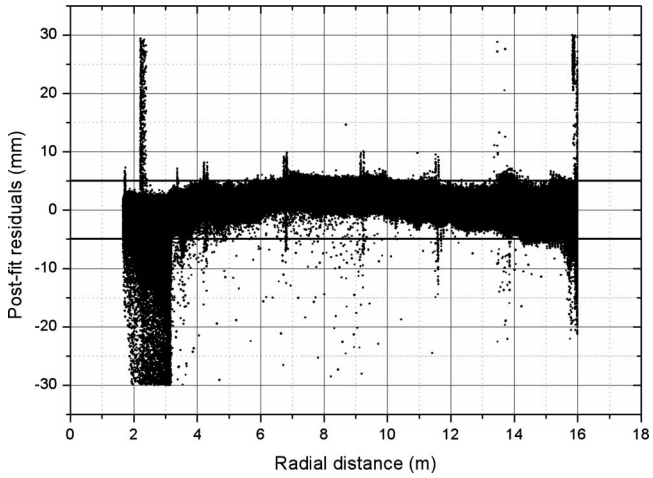

Fig. 7. Postfit residuals computed after the first adjustment as a function of the radial distance from the vertex; the threshold is 30 mm. Most of the points of the cloud have residuals values within the range $\pm$ 5 mm, identified by the black lines in the graph. Peaks are regularly visible as the radial distance from the vertex increases and they correspond to gaps between the panels.

software was written in Fortran 90 programming language (see next subsection) with the specific purpose to estimate the following six parameters:

- Three translations, required to transform the origin of the LS reference system (i.e., the instrument RP) in the vertex of the paraboloid;
- Two rotations, required to solve any misalignment between the axis of rotation of the paraboloid and the general (or primary) axis of the instrument; and
- The focal length of the best-fit paraboloid.

The postfit residuals were computed and used to perform data snooping and iteratively remove outliers from the merged point clouds. A first least-squares adjustment is computed adopting a threshold of 30 mm with the purpose of removing points that were not acquired on the primary mirror surface: its deformations are expected to be smaller than this threshold and any point having a larger postfit residual most probably does not belong to the primary reflector and it is removed from the point cloud. The postfit residuals' values obtained by point cloud adjustment at all antennas' elevations highlighted a common peculiar distribution, depending on the radial distance of the point from the vertex of the paraboloid (Fig. 7).

Most of the postfit residuals' values are contained in a 5-mm threshold. Nevertheless, bumps are clearly visible at particular radial distances that correspond to the locations of the gaps between the panels. These latter expose the underlying reticular structure to the LS beam and originate points that must be identified and removed from the cloud. Therefore, the second adjustment is performed with a more stringent threshold set at 5 mm; this value identifies the experimental survey's precision and determines the noise on the topology of the primary reflector as derived by the GS200 LS. It should be highlighted that such an overall performance of the LS is slightly worse (almost three times) but consistent with its nominal precision (see previous subsection). Degradation may be induced by the scattering properties of the primary reflector's paint and the occasionally severe incident angles of the line of sight.

For both telescopes, postfit residuals' standard deviations computed at a 5-mm threshold are shown in Table 1. The values

Table 1. Standard Deviations of the Postfit Residuals Distribution Are Computed at Different Elevations and Are Shown in Medicina and Noto Columns

Elevation (degrees)	Standard deviation of postfit residuals (mm) and efficiencies (in brackets)	
	Medicina	Noto
90	1.77 (0.68)	1.45 (0.77)
75	1.83 (0.66)	—
60	1.81 (0.67)	—
45	1.81 (0.67)	1.49 (0.76)
30	1.84 (0.66)	1.75 (0.68)
15	1.75 (0.68)	1.77 (0.68)

Note: For both telescopes, the corresponding efficiencies at 8.4 GHz are computed applying the Ruze's formula; the smaller values obtained for Noto's telescope suggest a better-fit of the physical shape of the primary reflector to an ideal rotational paraboloid.

determined for Noto are smaller and highlight a better adaptation of the data to a rotational paraboloid then in the case of Medicina. For the six elevation positions, the surface efficiency of the telescope at geodetic observing frequency (e.g., *X*-band 8.4 GHz), as determined from the LS data, can be computed inserting these standard deviations' values into the Ruze's formula (Ruze 1966); they are shown in bracket beside each corresponding standard deviation (Table 1). It is worth noticing that the efficiencies are lower than the efficiency experimentally measured at *X*-band for the two telescopes (>0.96): in our survey, the LS data are too noisy for an accurate determination of the topology of the two telescopes and cannot be used for metrology purposes (e.g., quantitative surface deformation investigation, active surface correction models and panels' alignment). Nevertheless, LS can be applied successfully to estimate the focal length values and its dependence on pointing elevation.

In order to define a common frame which all scanning could be referred to and all calculations and comparisons consistently performed, the translations and rotation angles obtained from different runs of the adjustment procedure were applied to the corresponding input data set (i.e., the complete point clouds at different elevations). The estimated rototranslation parameters were therefore used to transform the clouds into a cloud-related reference frame, thus transforming the instrument RP to the best-fit paraboloid vertex. The origins $O=(0,0,0)$ and the *Z*-axes (directed along the best-fit rotational axis) of the new frames algebraically coincide but may physically differ, i.e., the reference frames are realized similarly but do not share either the same orientation in space or the same origin. In fact, there is no part of the antenna structure that may be observed with the LS and may be considered fixed and suitable for defining the origin and orientation of a common reference system: all parts of the primary mirror undergo deformations. Therefore, the deformation patterns obtained through direct comparison of the LS data acquired at different antennas' pointing elevations should be regarded only as relative and not absolute patterns (the different frames might have residual misalignment along the *Z*-axes and origin translations). It is worth noticing that the orientation of *X* and *Y*-axes is defined by the LS; the continuous sequence of scanning performed from one standpoint ensures it is common for all elevations.

Under these specific limitations, the surfaces of the primary mirror as observed by the LS at six different elevations were compared one to another. It must be underlined that Noto active surface was deactivated in all scanning sessions, i.e., the main

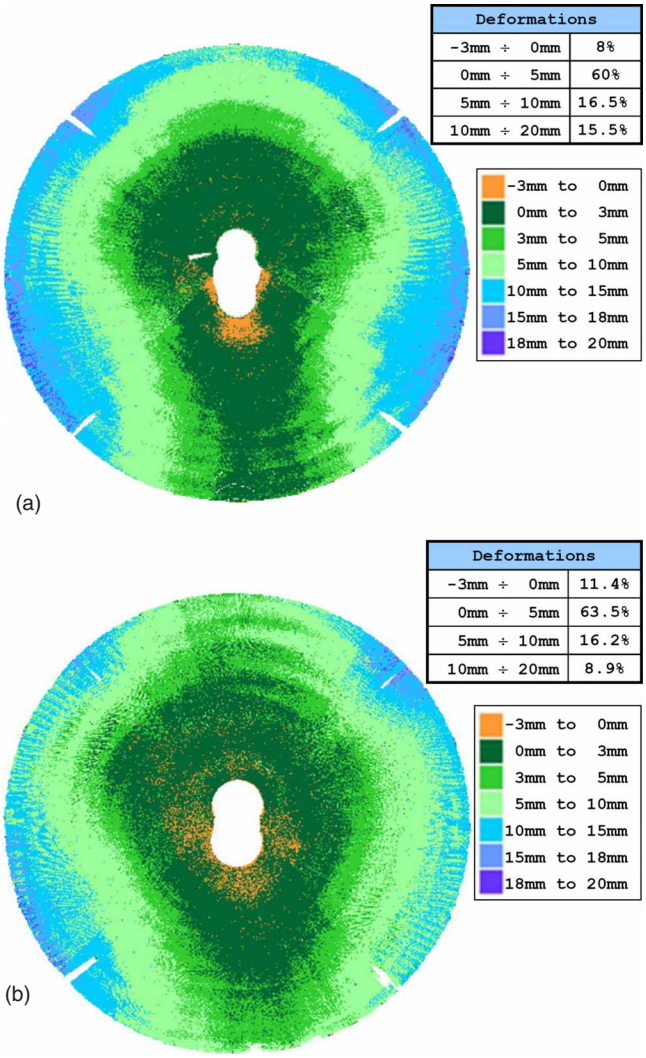

Fig. 8. Relative deformations of the dish between the scanning at 15° and the one at 90° for (a) Medicina; (b) Noto telescopes

reflector passively experiences the action of gravity at different elevation positions.

Fig. 8 shows the differences which are determined, for the telescopes of Medicina and Noto, when subtracting the 90° scanning session from the 15° scanning session. Similar comparisons were performed on all other remaining sets of points and creating all possible combinations of the scanning sessions acquired at different elevations. Qualitatively, the deformation patterns of the two telescopes are very similar: gravity induces a general inward folding of the dish as the elevation decreases. The deformations are almost symmetrical along the elevation axis (from left to right in Fig. 8) while the inward folding decreases in the lower part of the antenna (lower part of the dish in Fig. 8). This latter phenomenon is particularly intense on the Medicina telescope, as can be easily noticed by looking at the darker green color of Fig. 8. In general, the overall deformations computed for Noto are smaller. The differences between the surfaces of the primary mirror at 15° and 90° are within −3 mm and +5 mm for 68% of the scanned points in Medicina and 74% of scanned points in Noto; the points which are showing a deformation larger than 1 cm in Medicina are almost double than in Noto, with 15.5% and 8.9%, respectively. Summarizing, in terms of magnitude the deformations of Noto dish are slightly smaller than those computed at Medicina;

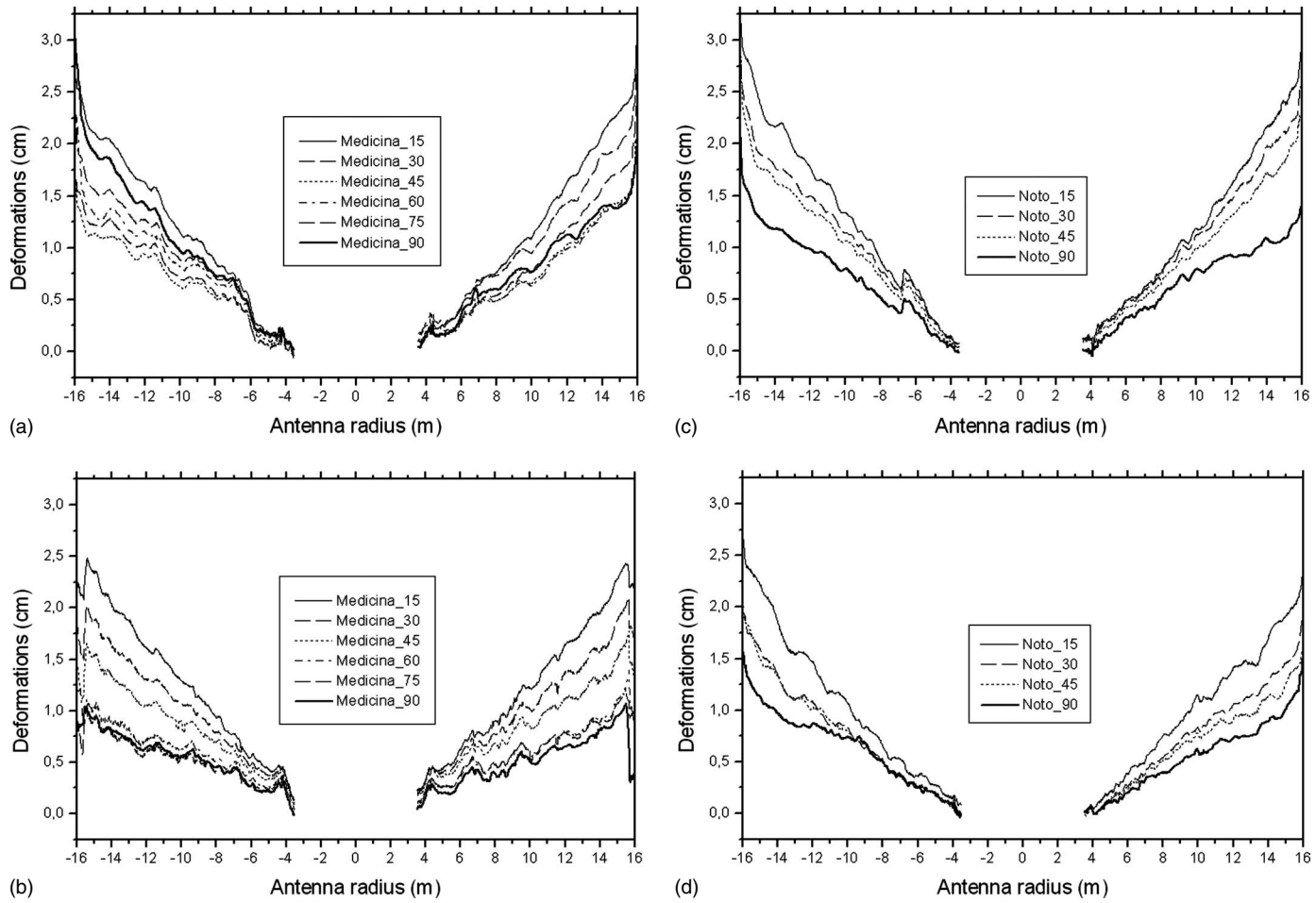

Fig. 9. (a), (b), (c), and (d): Transects of the deformations of the dish at different elevation across (a and c) and along (b and d) the elevation axis for the telescopes of Medicina and Noto. The deformations are obtained subtracting the theoretical rotation paraboloid (as designed in engineering projects) to the point clouds' grids interpolated at a 2 cm spacing.

this is probably due to a higher rigidity of the structure originated by the actuators that connect together and control the movements of the panels.

The magnitude and characteristics of the deformations of the dish are clearly and simply visualized considering normal sections of the paraboloid surface. The discrepancies between the reference primary mirror surface, namely the one corresponding to the nominal focal length $f_T=10.2590$, and the 2 cm grid computed using the local polynomial method (Yang et al. 2004) were computed for both telescopes and are shown in Figs. 9(a–d). Each grid was obtained by interpolating the scanned clouds expressed into the frame having origin in the vertex of the corresponding best-fit paraboloid, i.e., the scanned clouds whose points were rotated and translated by applying the best-fit angles and vectors estimated with the least-squares procedure described above. The planes $\pi_1: y=0$ and $\pi_2: x=0$ were intersected with the nominal paraboloid surface and the grids in order to compute sections; the orientations of the two coordinated planes are proximal to the parallel and orthogonal directions to the antenna elevation axis. For each direction, the project's design transects values were subtracted to the six grids' transects values.

The grids are totally independent from one another since they correspond to different scanning sessions. The inward folding of the dish is clearly visible by looking at the increasing differences between the nominal surface and the grids as the elevation decreases. Nevertheless, the way discrepancies evolve (as the radius increases) is also very similar for the six elevations: variations are similarly and accurately reproduced at all elevations suggesting that the LS effectively detects and determines primary mirror's roughness. A peculiarity can be highlighted for the Medicina primary mirror considering the sections contained into the plane $\pi_2: x=0$ [Fig. 9(b)]: all grids (i.e., all scanning) determine a deformation of the external panels which form the last and outer round. The discrepancies drop almost one-half of a cm for radius' values of $\cong$15.6 m and they are larger at higher elevations; the causes of such behavior remain unclear and will be further investigated.

The focal length value is tightly connected to the morphology of the primary mirror: it changes as the VLBI telescope moves in elevation. Particularly, an inward folding of the dish implies a decrease of the focal length. A focal length is associated to every scanned cloud with the least-squares procedure and it straightforwardly represents how intensely gravity folds the telescope structure (Fig. 10).

Again, the variation patterns are similar for the two telescopes and their trends are similar in sign and magnitude. As previously stated, due to the data loss that occurred in Noto, the focal lengths were not estimated at 60° and 75°. The focal length values estimated for both telescopes are listed in Table 2. The very large amount of points contained in each data set leads to an overoptimistic computation of standard deviations. The focal length's estimates tend to confirm a higher rigidity of Noto telescope. The

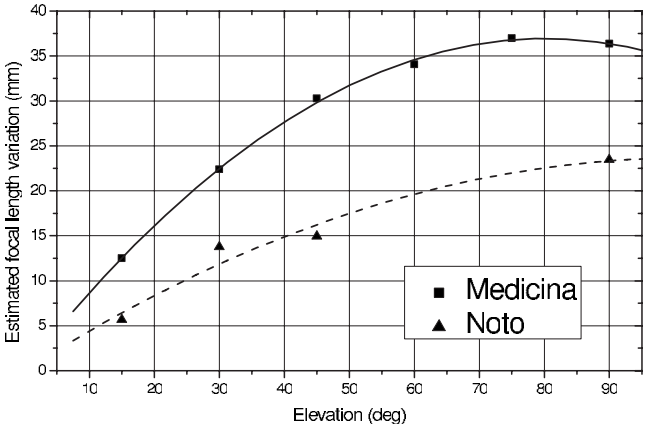

Fig. 10. Focal length variations estimated for Medicina and Noto telescopes as their pointing elevation changes

largest focal length difference is determined between the 90° and 15° positions: in Noto, it does not exceed 1.9 cm while in Medicina it is almost 2.5 cm.

Table 3 contains the differences between the theoretical focal length of the two telescopes $f_T=10.2590$ m and the values of Table 2. f_T is higher than any of the corresponding best-fit focal length values and the differences vary in the range of +(1.90–4.41) cm and +(2.24–4.06) cm for Medicina and Noto telescopes, respectively.

The best-fit procedure was also applied on the two separate clouds before the merging phase estimating a set of five transformation parameters for each scan and a common focal length. Therefore two rotation angles and three translations were estimated for each standpoint (F1 and F2) and a total of 11 parameters were derived for each elevation. In terms of the focal length's values this second approach is totally independent from the alignment phase realized on the overlapping scans and it does not highlight any significant discrepancy with the values obtained using the merged data set. Finally, in order to attempt to quantify the effects induced on the signal path length by the deformations of the primary mirror, the total path traveled by a planar wave front to a nominal focal point can be computed (Fig. 11).

For each point of the rototranslated cloud two distances are computed and summed: the first is the distance to the plane wave front, arbitrarily assumed to be $\pi: z=20$, and the second is the distance to the focal point $F_T=(0,0,10.259)$. In order to compute the average signal path at each elevation, it is important to take into consideration the uneven acquisition rate on the mirror surface. The whole area of the dish was acquired setting a sampling interval of 2 cm at a distance of 15 m; the central location of the

Table 2. Best-Fit Focal Length Values along with Their Formal Errors Estimated at Different Elevations

Elevation (degrees)	Focal length of the best-fit paraboloid (m)	
	Medicina	Noto
90	10.2403 ± 0.0001	10.2366 ± 0.0001
75	10.2410 ± 0.0001	—
60	10.2381 ± 0.0001	—
45	10.2342 ± 0.0001	10.2281 ± 0.0001
30	10.2264 ± 0.0001	10.2269 ± 0.0001
15	10.2165 ± 0.0001	10.2188 ± 0.0001

Table 3. Differences between Estimated Focal Lengths and Theoretical Focal Length for Medicina and Noto VLBI Telescopes

Theoretical focal length (m)	Elevation (deg)	Focal length differences (m)	
		Medicina	Noto
10.2590	90	0.0187	0.0224
	75	0.0180	—
	60	0.0209	—
	45	0.0248	0.0309
	30	0.0326	0.0321
	15	0.0425	0.0402

standpoints thus determines a denser acquisition on the inner part of the dish. Since the deformations of the primary mirror are uneven and increase toward the edge, a simple average of the distances computed on a generic cloud would lead to a biased estimate of the path due to the higher sampling rate of the inner (and more rigid) part of the dish. Twenty aureoles of equal area were therefore selected for each cloud and for each aureole averages were computed; the final unbiased signal path at each elevation could be computed averaging the 20 areal values. The signal path variations due to the deformations of the primary mirrors of the two telescopes are shown in Fig. 12: a second order polynomial function was fitted to the extra path lengths that were determined subtracting the shortest path (the one associated to the 15° elevation) from the others.

These path length variations are straightforwardly related to the gravitational deformations experienced by the primary mirror and they should thus be very close to the magnitude of the effect that the first addendum at the second member of (2) aims at describing. In order to compare these values, Fig. 12 also shows the values of $\alpha_f dF$ and the interpolating second order polynomial function for the two telescopes: the focal length variations are derived from Table 2 while, according to Clark and Thomsen (1988), the coefficient $\alpha_f=2-(8f^2/r_0^2)\ln(1+r_0^2/4f^2)$, can be evaluated as equal to 0.44, where f is the nominal focal length of the telescope and r_0 is its radius. The two curves are actually very similar for both telescopes: the LS can be efficiently used for a direct determination of the primary mirror folding and a rather straightforward assessment of the corresponding contribution to signal path variation.

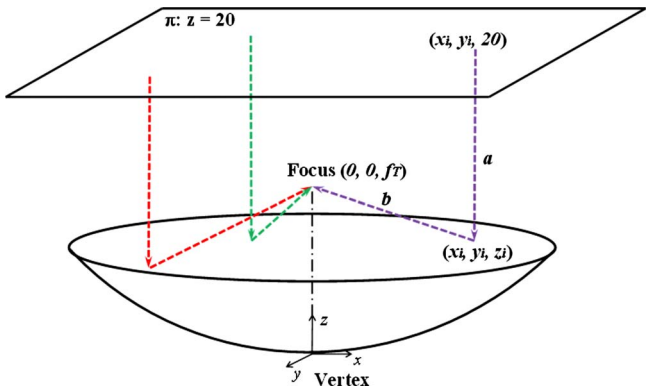

Fig. 11. Sketch of the signal path traveled by a point on the incoming planar wave front to the location of the focal point. For any point of the point cloud, the path can be computed as the sum of the moduli of the vectors $\vec{a}$ and $\vec{b}$.

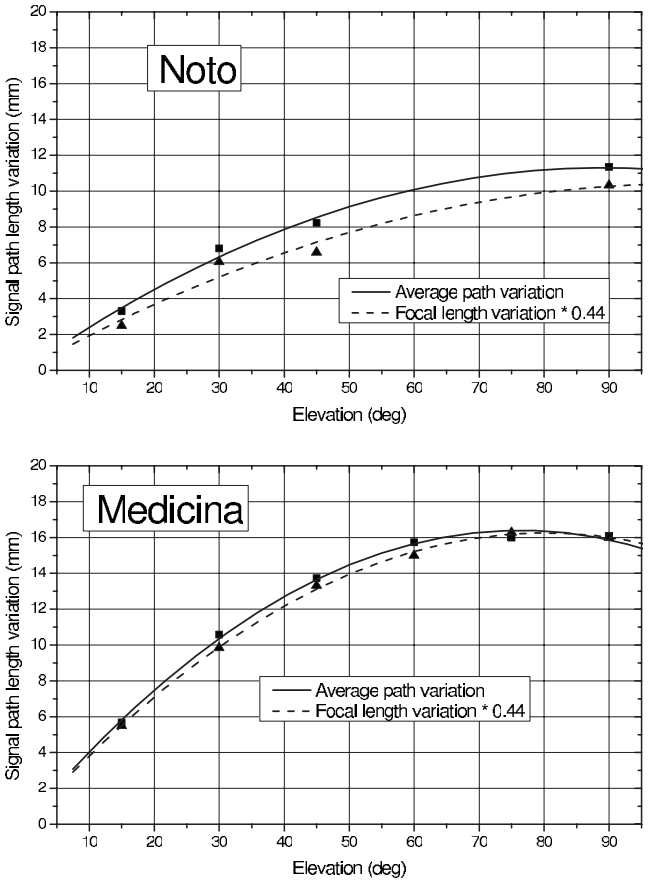

Fig. 12. Contribution of primary reflector deformations to signal path length variation: the two curves are obtained interpolating the signal path variations at four (six) elevation positions for Noto (Medicina) telescope according to Clark and Thomsen (1988) (triangle, dashed line) and to the direct computation of the signal path (see Fig. 11)

Best-Fit Paraboloid Software

The equation of the rotational paraboloid whose vertex is not located in the origin of the reference system is given by

$$(X' - X_V)^2 + (Y' - Y_V)^2 - 4f(Z' - Z_V) = 0 \tag{3}$$

where (X_V, Y_V, Z_V)=coordinates of the vertex.

In order to express Eq. (3) in a reference system with origin $O=(0,0,0)$ in the vertex, which is rotated by small angles $(d\Omega, d\Phi, dK)$ about the coordinate axes, the following transformation has to be applied

$$\begin{pmatrix} X' \\ Y' \\ Z' \end{pmatrix} = \begin{pmatrix} 1 & -dK & d\Phi \\ dK & 1 & -d\Omega \\ -d\Phi & d\Omega & 1 \end{pmatrix} \begin{bmatrix} X(i) \\ Y(i) \\ Z(i) \end{bmatrix} \tag{4}$$

where Ω=rotation around the x-axis; Φ=rotation around y-axis; K=rotation around Z-axis; $R=R_\Omega R_\Phi R_K$ expresses the linearized three-dimensional (3D) rotation matrix.

R aligns the original reference system defined by the instrumental RP and the instrument axis to the best-fit paraboloid. The primary mirror ideally represents a rotational paraboloid; the K angle around the Z-axis, being this latter the rotational axis, cannot be estimated and is set to zero. In case the angles are small, the coordinates in the new reference system are

$$X' = X(i) + Z(i)d\Phi$$

$$Y' = Y(i) - Z(i)d\Omega$$

$$Z' = -X(i)d\Phi + Y(i)d\Omega + Z(i) \tag{5}$$

Substituting Eq. (5) into Eq. (3) we obtain

$$[X(i) + Z(i)d\Phi - X_V]^2 + [Y(i) - Z(i)d\Omega - Y_V]^2 + 4f[-X(i)d\Phi + Y(i)d\Omega + Z(i) - Z_V] = 0 \tag{6}$$

where the unknowns are represented by three translations (X_V, Y_V, Z_V) needed to place the origin of the laser system in the vertex of the theoretical paraboloid, two rotations $(d\Phi, d\Omega)$ needed to solve any misalignment between the rotation axis of the paraboloid and the primary and secondary axis of the LS and by the focal length f of best-fit paraboloid.

Linearization of Eq. (6) gives

$$\begin{aligned} &2[X(i) + Z(i)d\Phi_a - X_a]\delta x_V + 2[Y(i) - Z(i)d\Omega_a - Y_a]\delta y_V \\ &+ 4f_a\delta z_V + 4[-X(i)d\Phi_a + Y(i)d\Omega_a + Z(i) - Z_a]\delta f \\ &- 2\{Z(i)[X(i) + Z(i)d\Phi_a - X_a] + 2X(i)f_a\}\delta\Phi \\ &- 2\{Z(i)[Y(i) - Z(i)d\Omega_a - Y_a] + 2Y(i)f_a\}\delta\Omega \\ &= [X(i) + Z(i)d\Phi_a - X_a]^2 + [Y(i) - Z(i)d\Omega_a - Y_a]^2 \\ &- 4f_a[-X(i)d\Phi_a + Y(i)d\Omega_a + Z(i) - Z_a] \end{aligned} \tag{7}$$

which in terms of matrices can be written as

$$\mathbf{A}\overline{\delta x} = \overline{f} + \overline{v} \tag{8}$$

where $\mathbf{A} \in M(m,6)$; $\overline{\delta x} \in (6,1)$; $\overline{f} \in (m,1)$; $\overline{v} \in (m,1)$; and m =number of points acquired by the LS. Eq. (8) can be solved with a classical least-squares approach for the scans performed at different elevations.

Terrestrial Surveys

Surveys Setup

The deformations determined with LS observations are expressed conformingly to a local reference system whose origin, according to computational requirements, can arbitrarily be located at e.g., the LS RP or the best-fit paraboloid vertex. The VLBI telescope RP is usually determined during a local tie by means of terrestrial observations, in particular triangulation, trilateration, and spirit leveling (see e.g., Johnston and Dawson 2004; Johnston et al. 2004), and is expressed with respect to a topocentric reference system. This latter serves as reference for other relevant parameters, e.g., coordinates of the markers of the local ground control network and the intertechnique eccentricity vector (in case a colocation is realized at the observing site). It is therefore convenient to express the LS derived deformations within the same topocentric system adopted for local ties operations.

The transformation between the laser specific reference system and the topocentric system can be realized, as usual, by means of surveying common points. In particular, the spheres installed at the edge of the dish (Fig. 5) were observed with a couple of total stations set up in the standpoints F1 and F2 (see Fig. 13); each sphere was coupled with a retroreflecting prism that could be turned and oriented so as to be visible and measurable from the pillars of the local ground control network, too.

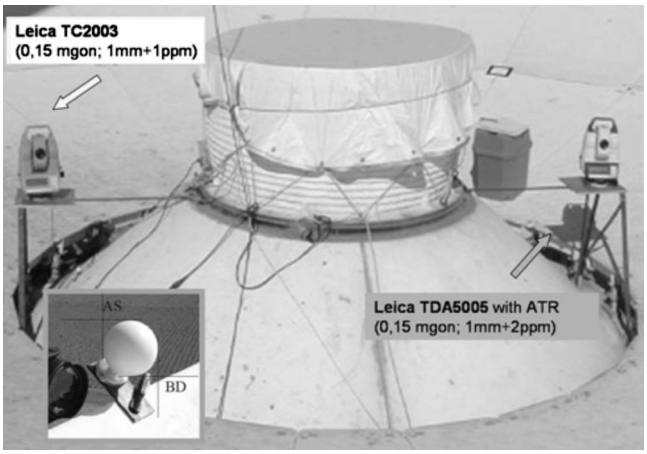

Fig. 13. Setup realized on the standpoints F1 and F2 through two total stations that measured the spheres and the retroreflecting prism (inset) used for connecting the laser scanning observations to the external local network

In order to locate the center of every sphere and to estimate its coordinates, the spheres were triangulated according to the observation scheme shown in Fig. 14. The symmetry of the objects was used to indirectly obtain measurements of angles that could be referred to the center: the zenith angle readings that were recorded by posing the horizontal cross-hair of the reticule tangentially to the upper and lower edge of the sphere, Z_u, and Z_l, respectively, could be averaged so as to obtain a zenith angle value referred to the center $\bar{Z}$. Analogously, left and right edges of the sphere were collimated using the vertical cross-hair of the reticule: the corresponding horizontal angles readings (A_l and A_r) were averaged so as to obtain an angle referred to the center of the sphere $\bar{A}$. The two averaged angles (zenith $\bar{Z}$ and azimuth $\bar{A}$) were used in the terrestrial observations' adjustment to estimate the centers of the spheres.

The centers of the spheres could be thus indirectly observed by triangulating from the two total stations. Contemporarily, the retroreflecting prisms beside each sphere were also observed by measuring angles and distances according to a forward intersection scheme. The resulting observing geometry is shown in Fig. 15, where the lines of collimation from F1 and F2 toward spheres

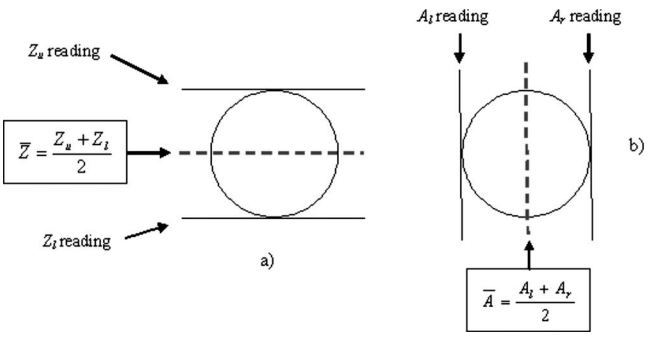

Fig. 14. (a) Collimation of the upper and lower edges of the spherical target using the horizontal cross-hair of the reticule; averaged zenith angle referred to the center $\bar{Z}$; (b) collimation of the lateral edges with the vertical cross-hair of the reticule; averaged azimuth angle of the center $\bar{A}$

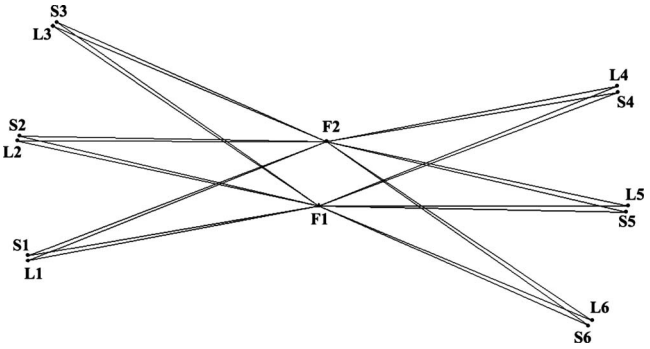

Fig. 15. Geometry of observations performed with the two total stations from F1 and F2 toward the six couples of targets spheres-prisms

and prisms are represented. The VLBI telescope's elevation position was held fixed at 90° during the observations.

The retroreflecting prisms were also collimated from the pillars of the local ground control network moving the VLBI telescope at the same elevations where the LS surveyed the primary mirror, i.e., 90°, 75°, 60°, 45°, 30°, and 15°.

Terrestrial Data Processing, Postprocessing, and Results

Distances, azimuth, and zenith angles acquired on the targets located on the edge of the dish and on the markers of the local ground control network were adjusted using "STAR*NET" software (Sawyer 2001). The geometry of the observations performed at Medicina is shown in Fig. 16: the collimation lines connect the targets and the standpoints.

The adjustment procedure allowed the estimation of the coordinates of the spheres within the topocentric system: the six prisms "*L*" and the six spheres "*S*" were observed at 90° from F1 and F2. The prisms were also observed from the local ground control network at all six VLBI telescopes' elevation steps. These latter observations establish the connections that are needed to insert the observations shown in Fig. 15 into the network of Fig. 16. The coordinates' standard deviations are shown in Table 4.

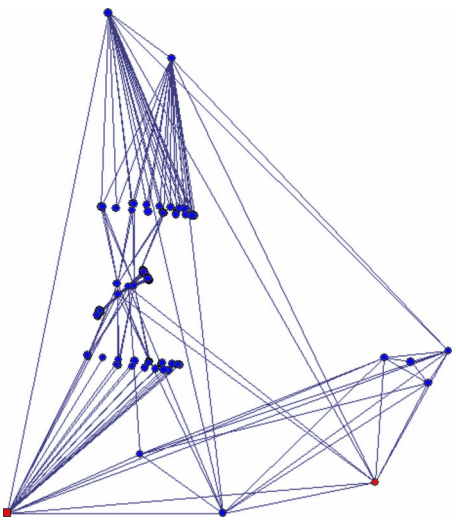

Fig. 16. Local ground control network is shown together with the standpoints F1 and F2 inside the dish and the retroreflecting prisms surveyed at six different elevations

Table 4. Marker Coordinates' Standard Deviations (Meters) Computed for the Medicina Terrestrial Survey

Marker name	X (m)	Y (m)	Elev (m)
F1	0.00049	0.00045	0.00044
F2	0.00049	0.00044	0.00044
L115	0.00073	0.00072	0.00066
L130	0.00072	0.00072	0.00068
L145	0.00072	0.00071	0.00069
L160	0.00071	0.00071	0.00070
L175	0.00070	0.00070	0.00071
L190	0.00068	0.00062	0.00055
L215	0.00071	0.00070	0.00068
L230	0.00070	0.00070	0.00069
L245	0.00070	0.00069	0.00070
L260	0.00069	0.00069	0.00070
L275	0.00067	0.00069	0.00070
L290	0.00055	0.00048	0.00047
L315	0.00070	0.00070	0.00071
L330	0.00069	0.00069	0.00071
L345	0.00068	0.00069	0.00071
L360	0.00067	0.00069	0.00071
L375	0.00065	0.00069	0.00071
L390	0.00058	0.00058	0.00055
L415	0.00060	0.00056	0.00058
L430	0.00060	0.00056	0.00058
L445	0.00060	0.00056	0.00059
L460	0.00060	0.00057	0.00059
L475	0.00061	0.00057	0.00059
L490	0.00055	0.00046	0.00046
L515	0.00061	0.00056	0.00056
L530	0.00061	0.00056	0.00057
L545	0.00060	0.00056	0.00057
L560	0.00060	0.00056	0.00058
L575	0.00060	0.00056	0.00058
L590	0.00056	0.00046	0.00046
L615	0.00061	0.00057	0.00054
L630	0.00061	0.00057	0.00055
L645	0.00060	0.00056	0.00056
L660	0.00060	0.00056	0.00057
L675	0.00060	0.00056	0.00058
L690	0.00055	0.00047	0.00046
S1	0.00177	0.00600	0.00234
S2	0.00109	0.00582	0.00220
S3	0.00309	0.00533	0.00229
S4	0.00171	0.00569	0.00222
S5	0.00104	0.00567	0.00215
S6	0.00303	0.00532	0.00228

Note: Letters F, L, and S, respectively identify standpoints, prisms (last two digits indicate VLBI telescope's pointing elevation), and spheres.

Table 4 shows that the standard deviations associated to Y coordinate of the spheres exceed half a centimeter; y-axis orientation is almost orthogonal to F1-F2 baseline. This large uncertainty originates from the geometry of the triangulation performed on the spheres. They were observed from standpoints F1 and F2 according to the approach illustrated in Fig. 14. The short baseline between the two standpoints ($\cong$3.4 m) heavily constraints the lines of sight toward the spheres in a very similar direction (see Fig. 15): observations along an orthogonal direction would have been valuable but they were not performed because no additional standpoints could be setup within the dish. The lack of trilateration measurements further complicates the problem: the total stations diastometers have a formal precision of 1 mm+1 ppm (TDA5005 0.2 mm for distances $<$120 m); distance measurements would have greatly reduced the positions' uncertainty along the line of sight (i.e., on the Y coordinate).

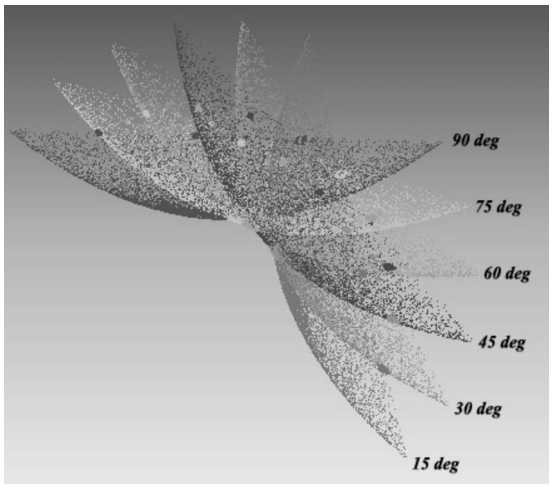

Fig. 17. Medicina scanning sessions framed and represented in the external reference system

Two similarity transformations are needed to transform the LS data and results into the local frame: (1) the topocentric coordinates of the spheres were used as common points to estimate the parameters of the similarity transformation which is needed to transform the laser clouds from their own system into the local system; (2) prisms' coordinates acquired at the six elevation positions were used for computing the similarity transformations' parameters between the 90° and the other pointing elevations of the VLBI dish. The parameters were applied to the clouds of points and to the vertex of the best-fit paraboloid [expressed in the local system according to previous step (1)] in order to transform each scan of the primary mirror into the local system at its corresponding position (Fig. 17). The large uncertainty on spheres centers and the two step transformation impact and degrade the precision associated to the vertex coordinates expressed into the local frame.

As previously stated, the centers of the spheres were independently estimated by means of the LS and the total stations' observations for the 90° VLBI dish's pointing position; the homothety factor of the similarity transformation computed using the coordinates of these two sets of points is $\tau = 1.0005 \pm 0.0002$. This value is estimated for both Medicina and Noto surveys; such a value cannot be explained in terms of antenna structure thermal expansion. The reference value of the thermal expansion coefficient of the antenna is $\alpha = 1.2 \times 10^{-5}\ C^{-1}$ and the time delay by which the antenna's structure responds to air temperature variations is $\Delta t = 2$ h (see e.g., Nothnagel et al. 1995). The temperature variations ΔT occurred between the LS and the topographic surveys are 2 and 10 C at Noto and Medicina, respectively. These temperature variations can cause an expansion of the structure which would explain a scale factor of $\cong$1.0001 for the Medicina survey; the effect of thermal expansion is expected to be five times smaller in Noto. Therefore, taking into account α, Δt, and ΔT, the scale factor between the two systems

cannot be explained and this discrepancy is most probably due to the electronic equipment of the LS, despite its magnitude is much higher than the nominal accuracy of the LS (1.5 mm at 50 m or 0.00003).

Discussions and Conclusions

The two twin 32-m AZ-EL VLBI telescopes located in Medicina and Noto were surveyed applying the same strategy with the aim to investigate gravitational deformation patterns that affect the primary mirror. Any variation of the morphology of the primary mirror straightforwardly influences the performances of the VLBI telescope since it modifies the signal path length. A convenient parameter that can be assumed to represent such variations is the focal length.

To this respect, LS surveying proves to be an innovative and effective method to monitor the elevation dependence on gravity of the focal length. For any possible pointing elevation of the telescope, LS allows a sufficiently precise estimate of the primary reflector deformations from which the related focal length can be estimated. Fig. 11 shows that the point clouds can also be used for a straightforward evaluation of the signal path variations caused by the primary mirror deformations.

We limited our investigation to six different elevation positions of the VLBI telescopes, obtaining consistent deformation patterns for both. The two structures react to gravity in a very similar manner; small differences can be highlighted in terms of deformations' magnitude. The VLBI telescope in Noto seems to have a more rigid primary mirror surface. The effect is most probably due to the presence of the actuators underneath the panels. Qualitatively, the structures react to gravity folding inwards as the line of sight turns from zenith to the horizon. This behavior is not perfectly symmetrical at the edge: the lower part of the dish experiences a weaker inward folding than the upper part.

The relative deformations of the surface could be quantified by combining the scans obtained at different elevations. The largest differences are found by subtracting the 90° to the 15° scans: 9% of the points in Noto and 15% in Medicina originate a difference which exceeds 1 cm.

The focal lengths and their variations could be estimated for both telescopes by using an ad hoc best-fit procedure on the LS data sets. Again, the variations are similar both in sign and magnitude. The inward folding of the dishes causes a shortening of the focal lengths, with a net variation of almost 2 cm for both telescopes. The difference between the nominal focal length (same for both telescopes) and the best-fit focal lengths at six different elevations could be computed: the experimental focal lengths are shorter for every position of the dish and the differences vary from 2 cm at zenith up to 4 cm at 15°.

If LS surveying efficiently determines and quantifies one of the three terms of Eq. (2) (the one related to focal length variations), the other two terms cannot be determined. The relative variations in the positions of the vertex and receivers as the elevation changes cannot be investigated with LS surveying.

An attempt to locate the scanned clouds of points in a local topocentric reference system, the one which serves as reference for local ties, was conducted by using triangulation and trilateration. Six retroreflecting targets were specifically installed on the edge of the dish and observed with a couple of total stations from the local ground control network. They were used as common points to compute the parameters of similarity transformations between the six relevant elevations of the telescopes: (90°, 75°, 60°, 45°, 30°, and 15°). These parameters were applied to the coordinates of the spheres' centers to transform the scanned clouds into the topocentric system. Unfortunately, the relatively large number of analytical computations required to complete the transformations degrade the accuracy of this specific task. Summarizing, the LS approach seems to completely fulfill the task of determining the focal length variations.

Acknowledgments

The writers thank M. Negusini for the precious help in performing the surveys and acquiring the data and G. Zacchiroli and A. Orfei for the useful conversations on the technical issues related to antennas performances. This paper is based on observations with the Medicina and Noto telescopes operated by INAF—Istituto di Radioastronomia.

References

Altamimi, Z., Collilieux, X., Legrand, J., Garayt, B., and Boucher, C. (2007). "ITRF2005: A new release of the international terrestrial reference frame based on time series of station positions and earth orientation parameters." *J. Geophys. Res.*, 112, B09401.

Besl, P. J., and McKay, N. D. (1992). "A method for registration of 3-d shapes." *IEEE Trans. Pattern Anal. Mach. Intell.*, 14(2), 239–256.

Carter, W. E., Rogers, A. E. E., Counselman, C. C., III, and Shapiro, I. (1980). "Comparison of geodetic and radio interferometric measurements of the Haystack-Westford base line vector." *J. Geophys. Res.*, 85, 2685–2687.

Clark, T. A., and Thomsen, P. (1988). "Deformations in VLBI antennas." *NASA Technical Memorandum 100696*, NASA, Greenbelt, Md.

Fröhlich, C., and Mettenleiter, M. (2004). "Terrestrial laser scanning-new perspective in 3D survey." *Proc., ISPRS Working Group VIII/2*, Institute for Forest, Albert Ludwigs Univ., Freiburg, Germany.

Gendt, G., Nothnagel, A., Pavlis, E., Lemoine, F., Van Dam, T., and Appleby, G. (2007). "Technique-specific biases and effects at co-location sites/satellites." *Unified analysis workshop 2007*, ⟨http://www.iers.org/documents/workshop2007/presentations/UAW_PosPap_Session_2_Dec02.pdf⟩ (Sept. 4, 2009).

Johnston, G., and Dawson, J. (2004). "The 2002 Mount Pleasant (Hobart) radio telescope local tie survey." *Geoscience Australia record 2004/21, 21*, ⟨http://www.ga.gov.au/geodesy/reports/localties/⟩ (Sept. 4, 2009).

Johnston, G., Dawson, J., and Naebkhil, S. (2004). "The 2003 Mount Stromlo local tie survey." *Geoscience Australia record 2004/20, 26*, ⟨http://www.ga.gov.au/geodesy/reports/localties/⟩ (Sept. 4, 2009).

Krügel, M., Thaller, D., Tesmer, V., Rothacher, M., Angermann, D., and Schmid, R. (2007). "Tropospheric parameters: Combination studies based on homogeneous VLBI and GPS data." *J. Geodesy, Berlin*, 81(6–8), 515–527.

Leinen, S., Becker, M., Dow, J., Feltens, J., and Sauermann, K. (2007). "Geodetic determination of radio telescope antenna reference point and rotation axis parameters." *J. Surv. Eng.*, 133(2), 41–51.

Nothnagel, A., Pilhatsch, M. and Haas, R. (1995). "Investigations of thermal height changes of geodetic VLBI radio telescopes." *Proc., 10th Working Meeting on European VLBI for geodesy and astrometry*, Agenzia Spaziale Italiana, Matera, Italy, 121–133.

Olmi, L., and Grueff, G. (2006). "SRT: Design and technical specifications." *Mem. S.A.It. Suppl.*, Vol. 10, J. Brand, K. -H. Mack, and I. Prandoni, eds., Istituto Nazionale di Astrofisica, Trieste, Italy, ⟨http://sait.oat.ts.astro.it/MSAIS/10/index.html⟩ (Sept. 4, 2009).

Orfei, A, Morsiani, M., Zacchiroli, G., Maccaferri, G., Roda, J. and Fiocchi, F. (2004). "An active surface for large reflector antennas." *IEEE Antennas Wireless Propag. Lett.*, 46(4), 11–19.

Pieraccini, M., Guidi, G., and Atzeni, C. (2001). "3D digitizing of cultural heritage." *J. Cultural Heritage*, 2, 63–70.

Ray, J., and Altamimi, Z. (2005). "Evaluation of co-location ties relating the VLBI and GPS reference frames." *J. Geodesy, Berlin*, 79(4–5), 189–195.

Rochblatt, J. D., and Seidel, L. B. (1992). "Microwave antenna holography." *IEEE Trans. Microwave Theory Tech.*, 40(6), 1294–1300.

Ruze, J. (1966). "Antenna tolerance theory—A review." *Proc. IEEE*, 54(4), 633–640.

Sarti, P., and Angermann, D. (2005). "Terrestrial data analysis and SINEX generation." *Proc., IERS Workshop on Site Co-Location*, Verlag des Bundesamts für Kartographie und Geodäsie, Frankfurt am Main, 118–127.

Sarti, P., Sillard, P., and Vittuari, L. (2004). "Surveying co-located space-geodetic instruments for ITRF computation." *J. Geodesy, Berlin*, 78(3), 210–222.

Sawyer, R. (2001). "STAR*NET-PRO V6 least-squares survey network adjustment." *Program reference manual*, Starplus Software, Inc., Oakland, Calif.

Schlüter, W., and Behrend, D. (2007). "The International VLBI service for geodesy and astrometry (IVS): Current capabilities and future prospects." *J. Geodesy, Berlin*, 81(6–8), 379–387.

Setti, G. (2006). "Synthetic history of the SRT project." *Mem. S.A.It. Suppl.*, Vol. 10, J. Brand, K. -H. Mack, and I. Prandoni, eds., Istituto Nazionale di Astrofisica, Trieste, Italy, ⟨http://sait.oat.ts.astro.it/MSAIS/10/index.html⟩ (Sept. 4, 2009).

Subrahmanyan, R. (2005). "Photogrammetric measurement of the gravity deformation in a Cassegrain antenna." *IEEE Trans. Antennas Propag.*, 53(8), 2590–2596.

Thaller, D., Krügel, M., Rothacher, M., Tesmer, V., Schmid, R., and Angermann, D. (2007). "Combined Earth orientation parameters based on homogeneous and continuous VLBI and GPS data." *J. Geodesy, Berlin*, 81(6–8), 529–541.

Tomasi, P. (1993). "Noto station status report." *Proc., IX Working Meeting European VLBI for Geodesy and Astrometry*, Geodaetischen Instituten der Rheinischen, Friedrich-Wilhelms-Universitaet, Bonn, Germany, 11–12.

Tomasi, P., et al. (1988). "The first geodetic VLBI experiment with the Bologna radio telescope." *Il Nuovo Cimento*, 11(2), 205–208.

Yang, C.-S., Kao, S.-P., Lee, F.-B., and Hung, P.-S. (2004). "Twelve different interpolation methods: A case study of Surfer 8.0." *Proc., XX ISPRS Congress*, IAPRS, Istanbul, Turkey, 778–786.

Yemez, Y., and Wetherilt, C. J. (2007). "A volumetric fusion technique for surface reconstruction from silhouettes and range data." *Comput. Vis. Image Underst.*, 105, 30–41.